

# Cooperative Micromanipulation Using Optically Controlled Bubble Microrobots

Kelly S. Ishii, *Student Member, IEEE*, Wenqi Hu, *Student Member, IEEE*, and Aaron T. Ohta, *Member, IEEE*

**Abstract**—Optically actuated bubbles in oil were used as microrobots. Simulations of the thermocapillary fluid flow within the oil phase are used to illustrate the mechanisms driving the bubble actuation. Parallel manipulation of sub-millimeter objects including glass beads and hydrogel beads was demonstrated. These capabilities show the potential for using the bubble microrobots in biomedical or other microassembly applications.

## I. INTRODUCTION

MICROROBOTS that are capable of micro-manipulation and microassembly have vast potential in furthering biomedical technology. One area of biomedical research that has gained much interest recently is the 3D culture of artificial tissues and organs *in vitro*. In 3D culture, cells are grown on a scaffold that mimics the natural extracellular matrix. Through the use of microfabrication techniques, small blocks of cell-laden scaffold called microgels can be created [1]-[3]. Acting as functional blocks of tissue, the microgels can be assembled into desired shapes or patterns, mimicking how groups of tissues are organized during tissue formation *in vivo* [2]-[4]. Of the several techniques used to assemble these microgels [2]-[8], only physical manipulation is capable of assembling specific individual microgels [5].

The use of wireless microrobots to physically manipulate and assemble microgels is a viable option. Current microrobotic systems utilize a diverse assortment of control and power delivery mechanisms, including electromagnetic [9]-[17], electrostatic [18], and optical actuation [19]. However, for a micromanipulation technique to be useful in many applications requiring microassembly, it is necessary to scale the system to process large numbers of objects. To achieve this, we focused on developing a system using multiple microrobots in parallel.

Existing systems that support the planar actuation of multiple microrobots in a common operating environment employ heterogeneous microrobot designs that selectively respond to a global control signal [16]-[18]. Frutiger *et al.* demonstrated the independent actuation of two frequency-selective microrobots that have mechanical responses at different resonant frequencies [16]. Time-division

multiplexing of the control signal enabled simultaneous, independent locomotion of two microrobots. Unique responses to different frequencies also allow the stick-slip microrobots of Floyd *et al.* to be selectively addressed [17]. Among a group of three microrobots, one could be independently addressed while the others moved in parallel. Structural variations in the steering arm of the scratch-drive actuated microrobots demonstrated by Donald *et al.* allowed individual addressing [18]. Assembly of up to four of these microrobots was demonstrated; however, further scaling is limited due to prohibitive voltage separation requirements and breakdown of the electrode insulation in the substrate.

In general, the techniques for decoupling microrobot responses to a single control signal require precise control systems and the tuning of individual microrobots. This can be challenging when expanding the number of microrobots in a system. In this paper, we describe a completely different approach to controlling multiple microrobots. Here, optical patterns are used to actuate sub-millimeter air bubbles in oil. Localized temperature gradients resulting from the conversion of the optical patterns to heat drive the motion of the bubble microrobots. Optical control is attractive due to the versatility of the “control signals” (light patterns) that can be produced and the relative ease of implementing this type of control system. Moreover, the system enables independent addressing of microrobots, actuation in series or parallel, and coupled or batch addressing. The bubble microrobots described here competed in the 2011 Mobile Microrobotics Challenge sponsored by the National Institute of Standards and Technology (NIST).

## II. MICROMANIPULATION SYSTEM

### A. Setup

The bubble microrobot control system utilizes computer-generated optical patterns projected onto the absorbent substrate of a microfluidic chamber to establish local temperature gradients (Fig. 1). Real-time visualization of the microrobots is provided via a microscope-mounted CCD camera connected to a computer. The control system is broken down into three components and described in further detail.

1) *Optical Patterns*: Light emitted from a modified computer projector (Dell 2400MP) serves as the source of the optical patterns. Different configurations are designed and animated in software, providing a versatile and affordable means for defining highly programmable control

Manuscript received September 16, 2011. This work was supported in part by the National Science Foundation, grant number EEC09-26632.

K. S. Ishii, W. Hu, and A. T. Ohta are with the Department of Electrical Engineering, University of Hawai'i at Manoa, Honolulu, HI 96822, USA (808-956-8196; fax: 808-956-3427; e-mail: aohta@hawaii.edu).

signals. Minimizing optics located beneath the microscope stage are used to focus the projector output on the absorbing substrate. The optical patterns are converted to heat by absorption in the substrate. The resulting thermal gradient is used to actuate the microrobot.

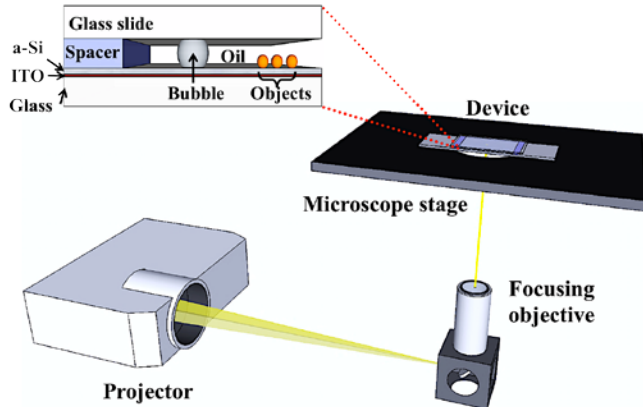


Fig. 1. Experimental setup. A fluidic chamber containing the microrobot(s) and other micro-objects rests on a microscope stage. An opening in the stage allows focused light patterns from the projector and optics beneath the stage to illuminate the device substrate.

2) *Microrobot Chamber*: The bubble microrobots are actuated in an enclosed microfluidic chamber built on top of the substrate. The optically absorbing substrate consists of a 1- $\mu\text{m}$ -thick layer of amorphous silicon (a-Si) coated over a 200-nm-thick layer of indium tin oxide (ITO) on a 1.1-mm-thick glass slide. Using an absorbing substrate reduces the light intensity required to cause an increase in the localized temperature. Empirical measurements show that a rise in temperature of approximately 1  $^{\circ}\text{C}$  can be achieved by with the projector as a light source.

The microfluidic chamber is composed of a glass slide bonded to the substrate. Spacers between the substrate and the glass slide define the height of the chamber. The assembled device is leveled on the microscope stage, as the bubbles will drift if any tilt is present.

3) *Control Software*: Various graphics were generated and controlled using programs written in Processing, an open source programming language and integrated development environment [20]. Running a program in the Processing development environment opens a window that displays the graphics specified within the code. Graphics defined within the Processing code can range from simple to complex; they can also be animated or be responsive to input from peripherals such as a mouse or keyboard. An image of the display window is sent to the projector, converting the graphics into optical patterns used to drive the microrobotic system.

The control programs used in the experiments presented in this paper create white circles of various diameters against a black background, maximizing contrast. Projecting one or more spots onto the substrate generates radial temperature gradients at the locations where the light is absorbed. The programs contain both predefined animations of circles traversing the display window as well as circles that can be moved by user input. The current control system does not

support feedback from the microscope, thus some user control is necessary. Currently, the control software relies on mouse and keyboard input to handle different events including spot generation, deletion, and movement.

### B. Theory and models

The bubble microrobots are driven by optically induced thermocapillary effects. This method of actuation has been demonstrated on gas bubbles in oil [21], [22]. When light patterns are focused onto an optically absorbent substrate, the light is converted to heat, establishing radial temperature gradients in the fluid. If a bubble is present, these temperature gradients generate surface tension gradients along the bubble interface and thermal Marangoni (thermocapillary) effects that give rise to fluid flow. As a result, a gas bubble in oil exhibits a net movement toward the region with the highest temperature, where it is then stably trapped. Vela *et al.* describes a second phenomenon, natural convection, as contributing to the flow, in work focusing on convection-based particle manipulation in water [23]. The natural convection alone produced forces similar to optical tweezers, but this is a different effect from the one described here. In the work by Vela *et al.*, fluid at the focal point of a 1480-nm laser reached a temperature near boiling. In the bubble microrobot system, light absorbed from the projector causes an approximately 1  $^{\circ}\text{C}$  increase. Therefore, the effect of natural convection is neglected, and the system is modeled on thermocapillary flow.

In previous work, the thermocapillary flow profile at the air-oil interface of a bubble was simulated using finite-element modeling software (COMSOL Multiphysics) [22]. The chamber was defined having height of 300  $\mu\text{m}$ . A fixed bubble with a 125- $\mu\text{m}$  radius was used. The light pattern was modeled as a saturated Gaussian heat distribution with a full-width at half-maximum of 424  $\mu\text{m}$  [24]. The peak temperature of the heat source was set to 300.8 K, matching the empirical value obtained when measuring light pattern incident on the substrate using a 50- $\mu\text{m}$  thermocouple element (Omega Engineering, Inc.). The boundary condition at the interface can be described by two equations:

$$\eta \left( \frac{\partial u}{\partial \mathbf{n}} \right) = \gamma_T \left( \frac{\partial T}{\partial \mathbf{t}} \right) \quad (1)$$

$$\gamma_T = \left( \frac{\partial \gamma}{\partial T} \right) \quad (2)$$

In equation (1),  $\mathbf{n}$  and  $\mathbf{t}$  are the unit vector normal and the tangent to the interface, respectively,  $\eta$  is the dynamic viscosity,  $u$  is the tangential component of the fluid velocity vector at the liquid/air interface, and  $T$  is the temperature [25]. Equation (2) is the derivative of the surface tension with respect to temperature, where  $\gamma$  is the surface tension [26].

Illuminating a point on the substrate with an optical pattern produces temperature gradients in both horizontal and vertical directions. Therefore, the simulation was broken down into two models describing the respective components of the fluid flow: parallel to the substrate, referred to as horizontal thermocapillary flow, and perpendicular to the substrate, or vertical convective flow. In the following

simulations, a fixed air bubble is treated as the frame of reference. The bubble is static and flow-induced deformation is not considered. Empirical observations have shown that the bubble makes a contact angle of  $180^\circ$  with the substrate. Although the simulation describes the flow profile around a single bubble, parallel bubble actuation has been verified experimentally.

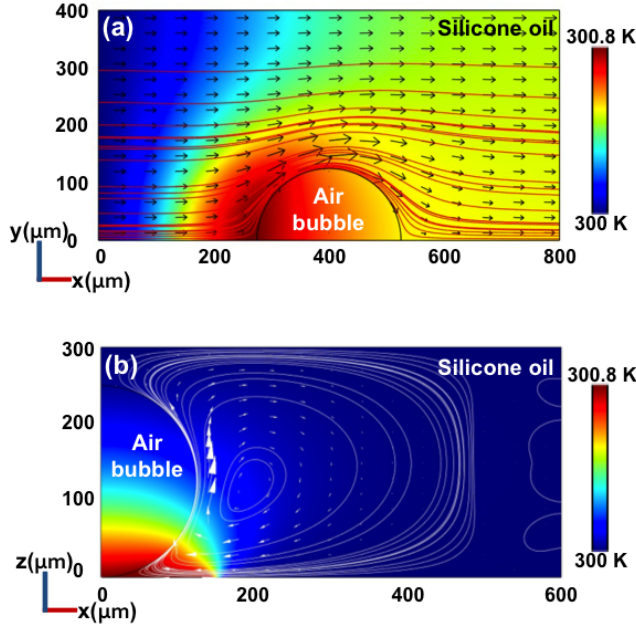


Fig. 2. Simulations of the thermocapillary flow around a stationary air bubble. (a) A heat source at one end of the bubble produces a temperature gradient along the air-oil interface, causing horizontal thermocapillary flow. (b) The same heat source in (a) positioned at the center of the bubble induces vertical convective flow, shown in this side view of the fluidic chamber.

Using a heat source with maximum temperature at  $x = 250 \mu\text{m}$ , the simulation of horizontal thermocapillary flow illustrates how temperature and surface tension gradients drive horizontal fluid flow from the heated side of the bubble to the cooler side (Fig. 2a). As a result of the flow, the bubble exhibits a net movement toward the heat source. The motion of the bubble will cease when it is centered at the maximum of temperature gradient.

The vertical convective flow is caused by the temperature gradient that extends upward from the substrate to the surface of the fluidic chamber. This flow is present in the fluid surrounding the heated bubble, even when the bubble is centered about the heat source. The vertical convective flow is normal to the substrate near the bubble interface, but is part of a larger circulatory flow (Fig. 2b). Objects that have a higher density than the liquid phase can be pulled toward the bubble by the convective flow. These objects will remain stably trapped near the bubble as long as the vertical convective flow force is less than the gravitation force. Conversely, objects that are less dense than the fluid end up following the circulatory flow, and can be repelled, as observed in experiments involving hydrogel beads.

### C. Fabrication

1) *Fluidic Chamber*: Two chamber designs were used in the experiments presented in this paper; the first was built to address the requirements of the NIST Mobile Microrobotics Challenge, whereas the second is a more generalized design that was used to demonstrate additional capabilities of the microrobot.

The first chamber consists of a 1.1-mm-thick glass slide bonded to the a-Si substrate with 300- $\mu\text{m}$ -thick spacers separating the layers. Epoxy (Devcon, Illinois Tool Works Inc.) was used as the bonding agent and a stack of three glass cover slips formed the spacers. The chamber is opened as only the two sides where the spacers are located are sealed with epoxy. At the open ends, carrier fluid is introduced to the chamber by capillary flow. The height of the chamber also provides sufficient room for insertion of a thin syringe tip and micro-objects. For the final devices used during the microrobotics competition, arena structures were patterned onto the substrate before the chamber was assembled.

The more rigid design of the epoxy chamber was desirable to ensure that height requirements were met and to help with transportation. Although the chamber can be reused, it eventually accumulates enough dust and other unwanted particles that the microrobot performance suffers. The microrobot movement is sensitive to particles on the surface of the substrate. Cleaning the substrate is difficult for the epoxied fluidic chamber since it cannot be disassembled once the epoxy cures.

A second, simpler chamber design enables better reuse of the substrate across multiple experiments due to the lack of a permanent bond. This chamber is similarly built: a-Si-coated glass serves as the substrate; a glass coverslip replaces the glass microscope slide as the chamber cover; and two sides of the chamber are left open-ended. Instead of cover slips, the spacers consist of three layers of double-sided tape. The tape provides a way to fix the height of the chamber and also creates a seal between the layers. The tape adhesive provides a useable, but weaker seal; therefore the device should be reassembled frequently. Reassembly coincides with the need to clean the substrate of debris and does not take much effort.

2) *Bubble Microrobot*: The microrobot used in this system consists of an air bubble in oil. Bubbles are introduced into the chamber by extruding a small amount of air into the oil from a syringe. In order to place the bubble past the raised walls of the arena it was necessary to use a syringe tip that was thin enough to be inserted over the walls. To release the bubbles, tilting the chamber at an angle so that the open end is elevated and shaking it a bit will cause the bubbles to rise and exit the oil.

3) *Arena*: Based on specifications from NIST, two arena layouts were drawn to scale in AutoCAD and used to create transparency photomasks. To fabricate the arena structures in the chamber, the a-Si substrate was first cleaned with a serial wash of acetone, methanol, isopropyl alcohol (IPA),

and deionized water. After cleaning, the substrate was spin-coated with SU-8 photoresist (MicroChem Corp.) to a thickness of 50  $\mu\text{m}$ . Next, the SU-8 was sequentially pre-baked, soft-baked and exposed under a mask aligner according to product specifications. It then underwent a post-exposure bake before developing for approximately six minutes with MicroChem SU-8 developer. The developer was removed with IPA coupled with light agitation and the remaining structures were blow-dried with nitrogen before undergoing a final hard-bake.

4) *Micro-objects*: Various sub-millimeter objects of different materials and geometries were used to test the manipulation capabilities of the microrobot. These include glass beads, polymer-based triangle blocks, and hydrogel beads containing yeast cells.

The second task for the 2011 Mobile Microrobotics Challenge involved packing triangular blocks within an “alley,” or a narrower section of a T-shaped arena. Right triangle blocks with legs of 360  $\mu\text{m}$  and 185  $\mu\text{m}$  were fabricated from SU-8 in a modified version of the arena fabrication procedure described above. Here, a silicon wafer was used instead of the a-Si substrate. The SU-8 was spin-coated at an average thickness of 100  $\mu\text{m}$ , and was developed for approximately ten minutes. To retrieve the triangle pieces, the wafer was sprayed with IPA, removing the undeveloped SU-8 and dislodging the triangles.

Hydrogel beads containing yeast were also fabricated and tested. Agarose is a biocompatible, thermoresponsive hydrogel that is commonly used in cell culture. The agarose provides a protective buffer for the cells during manipulation. A solution of 1.5% (w/w) low-melting-point agarose (Promega) in deionized water was prepared. Powdered agarose mixed with water was heated in a microwave for one to two minutes until the agarose was completely dissolved. The solution was reweighed and adjusted for water lost through evaporation during the microwaving.

Bakers’ yeast was rehydrated and mixed into agarose solution that had been cooled to approximately 30°C. The agarose-yeast mixture was then added to chilled Fluorinert™ FC-40 oil (3M Corp.) and shaken to form a droplet emulsion. To form beads, the temperature of the solution was quickly dropped below the gelling point of the agarose (24 to 28°C) by refrigerating for approximately five minutes. Bead samples could then be retrieved by pipet.

### III. RESULTS

#### A. Glass Beads

The force produced by bubble microrobots on a 60- $\mu\text{m}$ -radius glass bead in silicon oil was measured (Fig. 3). Glass beads are denser than the oil, so they sink to the bottom of the chamber. Two mechanisms for manipulating the beads were observed, referred to here as pulling and pushing modes. In the pulling mode, the bead becomes trapped in the vertical convective flow at the base of the bubble, pulling it inwards toward the bubble. In this mode, the bead does not

have to be in direct contact with the bubble meniscus since the circulatory flow extends outward into the oil surrounding the bubble. Conversely, in the pushing mode, the bead is continuously in contact with the bubble, and is moved by the bubble meniscus.

The effect of increasing the radius of the bubble while maintaining the light pattern at a constant size was examined. The force exerted on the glass bead was calculated using Stokes’ Law. Friction with the surface is not taken into account, so the actual force produced on the bead by the bubble microrobot is likely larger than the values shown here (Fig. 3). The pushing and pulling forces increase until they reach a maximum for bubble radii between 100 and 200  $\mu\text{m}$ . The decrease in force for larger bubbles can be partly attributed to the decrease in actuation velocity as bubbles of larger size are used.

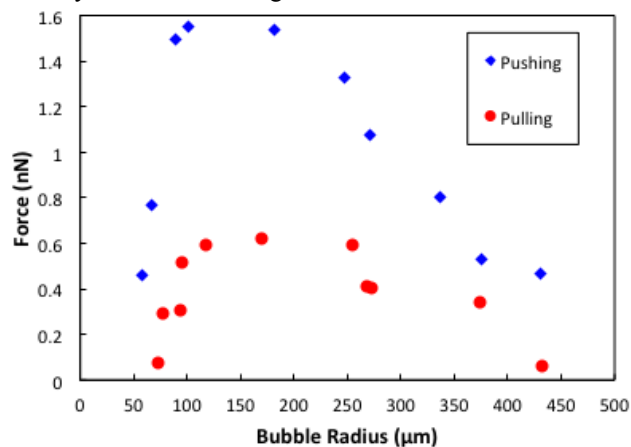


Fig. 3. Relationship between the average force exerted on a glass bead and the radius of the bubble microrobot. The radius of the bead being manipulated was 60  $\mu\text{m}$ . The average light intensity of the optical patterns was 5.3  $\text{W}/\text{cm}^2$  and the light pattern radius was 140  $\mu\text{m}$ .

#### B. Microassembly of SU-8 Triangles

During the 2011 Mobile Microrobotics Challenge, the bubble microrobot was able to move two SU-8 triangle blocks from the starting area into the alley, but did not accomplish the goal of tightly packing the them within the allotted time. The manipulation and tight packing of three of the SU-8 triangles over the course of six minutes was presented in a separate work [22]. As the SU-8 blocks are denser than silicone oil, they settle on the bottom of the chamber rather than float. Friction can be a problem when the interior of the chamber becomes too dirty; the microrobot or other micro-objects can become stuck, or have their motion impaired. The problem of friction is likely exacerbated by the coarseness of the triangles’ surfaces resulting from the fabrication process.

#### C. Parallel Actuation and Microassembly

One application of the bubble microrobots introduced in previous work was microassembly of hydrogel beads using a single bubble [22]. Parallel actuation of three microrobots was also demonstrated, although the microrobots were not manipulating any micro-objects. Here, parallel actuation of multiple microrobots is further explored, and subsequently



combined with microassembly techniques to demonstrate cooperative microassembly.

Multiple microrobots can be actuated in close proximity to one another. Six microrobots were simultaneously actuated using keyboard controls, with groups of three assigned to a single set of controls (Fig. 4). Although it is possible to independently operate each of the microrobots, the task of independent and simultaneous manual control becomes increasingly difficult with many microrobots. In the current system, the ability to simultaneously address individual microrobots can be achieved one of two ways: by using predefined moving light patterns or by manual control of the light patterns using keyboard inputs. The former method was used in the previous demonstration of parallel actuation [22]. The latter method requires that enough sets of unique keys are available to control microrobot movement. Furthermore, a single user can only actuate two independent microrobots at the same time and still be able to use them purposefully.

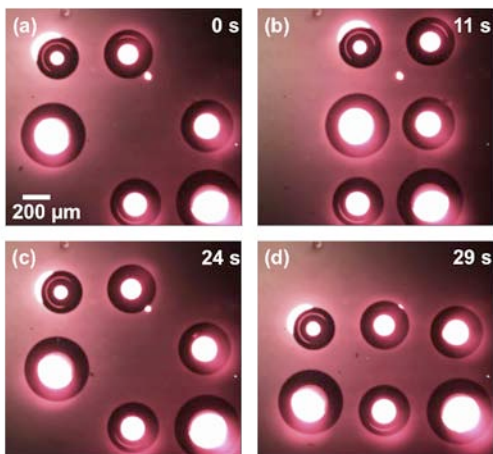


Fig. 4. Six microrobots are manipulated in parallel. Groups of three microrobots assigned to a single set of controls (a) are moved together forming a 2x3 array (b). The groups are returned to their original configuration (c) and moved together again, this time into a 3x2 array (d).

Two independently controlled microrobots were cooperatively actuated to arrange yeast-laden agarose beads (Fig. 5). In this experiment a separate person controlled each microrobot using keyboard inputs. The agarose beads are less dense than the carrier fluid, allowing them to float. According to the vertical convection flow model, the floating beads are in the region where convective flow is circulating away from the bubble interface. However, the beads are large enough that they are not continuously circulated in the convection, and are instead repelled by the flow surrounding the bubble microrobots.

Initially, the microrobots were used to clear a region of extraneous beads. The microrobots were positioned on opposite sides of a small group of beads (Fig. 5a), and then moved toward each other to maneuver the beads into a horizontal line two beads wide (Fig. 5b). The microrobots then rotated the line of beads 90° counterclockwise (Fig. 5c-5d). The bubbles were then brought closer together and

moved along the line, straightening the beads into a single-file line (Fig. 5e-5f).

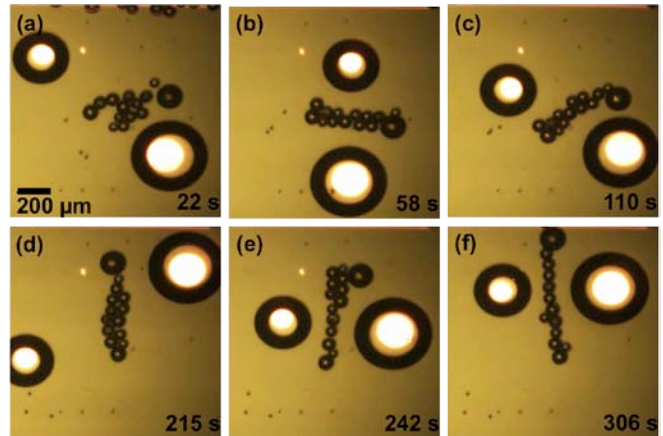


Fig. 5. Manipulation of a sample of agarose beads containing yeast using two independently controlled bubble microrobots. The initial cluster of beads (a) was pushed into a horizontal line (b), then rotated 90° (c-d). Moving the bubbles along the beads straightened them into a single-file line (e-f). The small bright dot in the photos is the projection of the mouse cursor onto the device and the tiny black flecks are stray yeast.

Three microrobots were used in parallel to perform a cooperative bead "handoff" routine (Fig. 6). The upper and lower microrobots were independently controlled by keyboard while the central microrobot followed an automated path traveling from left to right and back again along a horizontal line. In a combination of pushing and pulling modes, a single glass bead was passed between the bubbles, following a sequence of middle-top-bottom-middle.

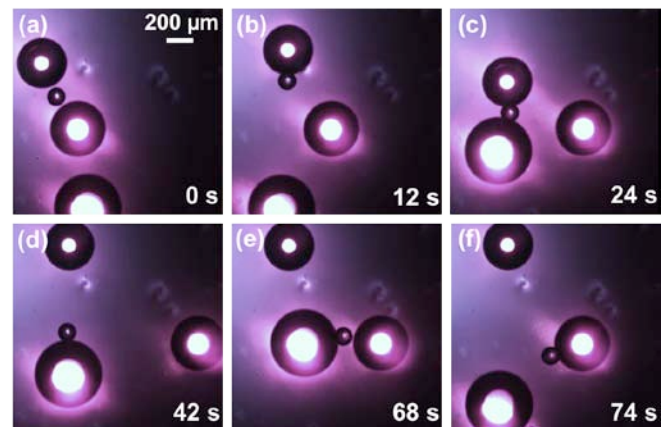


Fig. 6. A 66- $\mu\text{m}$ -radius glass bead is passed between three independently controlled microrobots. The bead is passed from the middle to the top microrobot (a-b), from the top to the bottom (c-d), and from the bottom back to the middle (e-f).

#### IV. DISCUSSION

Empirical results show that both pushing and pulling modes can be used to manipulate objects with a density greater than the carrier fluid. This can be useful for obstacle navigation, correction during microassembly tasks, or in cooperative microassembly. When the objects under manipulation are less dense and float, as in the case of agarose beads in FC-40, only the pushing mode is observed.

Unlike the pushing mode exhibited in the glass bead and triangle manipulation, the agarose beads remain at a minimum distance from the bubble at all times.

Advantages of the bubble microrobot system include relatively few hardware requirements, uncomplicated microrobot and platform fabrication, and a straightforward, graphics-based approach to control software. This system is unique in that the microrobot itself does not require special material, just air. New microrobots are generated on-demand and can be replaced indefinitely.

To expand to larger scale operation, the system can be improved in a number of ways. Limitations of the bubble microrobots were primarily related to the behavior of air bubbles in carrier fluid. One problem is variation in bubble size. Extrusion of air through a fine-tipped syringe is currently used since it does not require any specialized equipment. The drawback of this method is inconsistency in bubble size, evident in the parallel actuation images. Adoption of an alternative method that offers increased precision should be considered. Another problem arises when solid structures render bubbles immobile. Rough walls, substrate defects, and debris are all possible structures that can cause a bubble to become stuck. Additionally, the formation of bubble microrobots can only occur with carrier fluids that have enough surface tension to maintain bubbles for reasonable amounts of time.

## V. CONCLUSION

In this paper we further explored the capabilities of optically actuated bubble microrobots. Actuation has been demonstrated in two types of oil and manipulation of three types of micro-objects was accomplished. The ability to have multiple microrobots working in parallel is a benefit of this system. Here we have presented independent, simultaneous control of multiple microrobots within close proximity of each other, and have used this technique to show two microrobots working in unison to assemble hydrogel beads.

Future work includes the development of autonomous control using image feedback integrated with the control software, and characterization of the dynamics of the multiple-bubble system. Related work pursued in parallel and published separately involves the manipulation of micro-objects in aqueous fluidic environments using laser-driven bubbles, thus improving compatibility with biomedical applications [27].

## ACKNOWLEDGMENT

The authors would like to thank Dr. Xiaoxiao Zhang and Dr. David Garmire for helpful discussions.

## REFERENCES

[1] Y. Ling, *et al.*, "A cell-laden microfluidic hydrogel," *Lab Chip*, vol. 7, pp. 756-762, 2007.  
 [2] Y. A. Du, E. Lo, S. Ali, A. Khademhosseini, "Directed assembly of cell-laden microgels for fabrication of 3D tissue constructs," *Proc. Natl. Acad. Sci. USA*, vol. 105, pp. 9522-9527, 2008.

[3] A. Khademhosseini, R. Langer, "Microengineered hydrogels for tissue engineering," *Biomater.*, vol. 28, pp. 5087-5092, 2007.  
 [4] Y. Du, *et al.*, "Surface-directed assembly of cell-laden microgels," *Biotechnol. Bioeng.*, vol. 105, pp. 655-662, 2009.  
 [5] J. Yeh, *et al.*, "Micromolding of shape-controlled, harvestable cell-laden hydrogels," *Biomater.*, vol. 27, pp. 5391-5398, 2006.  
 [6] V. L. Tsang, *et al.*, "Fabrication of 3D hepatic tissues by additive photopatterning of cellular hydrogels," *FASEB J.*, vol. 21, pp. 790-801, 2007.  
 [7] Y. Du, E. Lo, M. K. Vidula, M. Khabiry, A. Khademhosseini, "Method of bottom-up directed assembly of cell-laden microgels," *Cell. Mol. Bioeng.*, vol. 1, pp. 157-162, 2008.  
 [8] B. Zamanian, *et al.*, "Interface-directed self-assembly of cell-laden microgels," *Small*, vol. 6, pp. 937-944, 2010.  
 [9] L. Zhang, J. J. Abbott, L. Dong, B. E. Kratochvil, D. Bell, and B. J. Nelson, "Artificial bacterial flagella: Fabrication and magnetic control," *Appl. Phys. Lett.*, vol. 94, p. 064107, 2009.  
 [10] G.-L. Jiang *et al.*, "Development of rolling magnetic microrobots," *J. Micromechanics and Microeng.*, vol. 20, p. 085042, 2010.  
 [11] M. S. Sakar, E. B. Steager, D. H. Kim, M. J. Kim, G. J. Pappas, and V. Kumar, "Single cell manipulation using ferromagnetic composite microtransporters," *Appl. Phys. Lett.*, vol. 96, p. 043705, 2010.  
 [12] M. S. Sakar, E. B. Steager, A. Cowlet, V. Kumar, and G. J. Pappas, "Wireless manipulation of single cells using magnetic microtransporters," *Proc. IEEE Int. Conf. Robot. Autom. (ICRA)*, pp. 2668 - 2673, May 2011.  
 [13] W. Jing *et al.*, "A magnetic thin film microrobot with two operating modes," *Proc IEEE Int. Conf. Robot. Autom. (ICRA)*, pp. 96-101, May 2011.  
 [14] I. A. Ivan *et al.*, "First experiments on MagPieR: A planar wireless magnetic and piezoelectric microrobot," *Proc. IEEE Int. Conf. Robot. Autom. (ICRA)*, pp. 102-108, May 2011.  
 [15] S. Palagi *et al.*, "Design and development of a soft magnetically-propelled swimming microrobot," *Proc. IEEE Int. Conf. Robot. Autom. (ICRA)*, pp. 5109-5114, May 2011.  
 [16] D. R. Frutiger, K. Vollmers, B. E. Kratochvil, and B. J. Nelson, "Small, fast, and under control: wireless resonant magnetic microagents," *Int. J. Robot. Res.*, vol. 29, pp. 613-636, 2009.  
 [17] S. Floyd, E. Diller, C. Pawashe, and M. Sitti, "Control methodologies for a heterogeneous group of untethered magnetic micro-robots," *Int. J. Robot. Res.*, vol. 30, pp. 1553-1565, 2011.  
 [18] B. R. Donald, C. G. Levey, and I. Paprotny, "Planar microassembly by parallel actuation of MEMS microrobots," *J. Microelectromech. Syst.*, vol. 17, pp. 789-808, 2008.  
 [19] O. J. Sul, M. R. Falvo, R. M. Taylor, S. Washburn, and R. Superfine, "Thermally actuated untethered impact-driven locomotive microdevices," *Appl. Phys. Lett.*, vol. 89, pp. 203512, 2006.  
 [20] Processing.org, last accessed: Sep. 16, 2011. [Available]: <http://processing.org/>  
 [21] A. T. Ohta, A. Jamshidi, J. K. Valley, H.-Y. Hsu, and M. C. Wu, "Optically actuated thermocapillary movement of gas bubbles on an absorbing substrate," *Appl. Phys. Lett.*, vol. 91, pp. 074103, 2007.  
 [22] W. Hu, K. S. Ishii, and A. T. Ohta, "Micro-assembly using optically controlled bubble microrobots," *Appl. Phys. Lett.*, vol. 99, pp. 094103, 2011.  
 [23] E. Vela *et al.*, "Non-contact mesoscale manipulation using laser induced convection flows," *IEEE/RSJ Int. Conf. Intel. Robot. Syst. (IROS)*, pp. 913-918, Sept. 2008.  
 [24] S. L. Neale, A. T. Ohta, H.-Y. Hsu, J. K. Valley, A. Jamshidi, and M. C. Wu, "Trap profiles of projector based optoelectronic tweezers (OET) with HeLa cells," *Opt. Express*, vol. 17, pp. 5231, 2009.  
 [25] V. G. Levich, "Physicochemical Hydrodynamics," Prentice-Hall, Inc., Englewood Cliffs, N. J., 1962.  
 [26] E. Lajeunesse and G. M. Homsy, "Thermocapillary migration of long bubbles in polygonal tubes. II. Experiments," *Phys. Fl.*, vol. 15, pp. 308, 2003.  
 [27] W. Hu, K. S. Ishii, and A. T. Ohta, "Micro-assembly using optically controlled bubble microrobots in saline solution," *2012 IEEE Int. Conf. Robot. Autom. (ICRA)*.